Molecular dynamics simulation of deformation behavior in amorphous polymer: nucleation of chain entanglements and network structure under uniaxial tension

Yashiro, Kisaragi

Ito, Tomohiro

Tomita, Yoshihiro

(Citation)
International Journal of Mechanical Sciences,45(11):1863-1876

(Issue Date)
2003-11

(Resource Type)
journal article

(Version)
Accepted Manuscript

(URL)
https://hdl.handle.net/20.500.14094/90000012

Molecular dynamics simulation of deformation behavior in amorphous polymer: Nucleation of chain entanglements and network structure under uniaxial tension

Kisaragi Yashiro [a,*] Tomohiro Ito [b] Yoshihiro Tomita [c]

[a] *Department of Mechanical Engineering, Faculty of Engineering, Kobe University, Rokkodai, Nada, Kobe 657-8501, Japan*

[b] *Student of Graduate School of Science and Technology, Kobe University, Rokkodai, Nada, Kobe 657-8501, Japan*

[c] *Graduate School of Science and Technology, Kobe University, Rokkodai, Nada, Kobe 657-8501, Japan*

Abstract

In order to clarify the mechanical behavior of molecular chains in amorphous polymers, a molecular dynamics simulation is conducted on a nanoscopic specimen of amorphous polyethylene under uniaxial tension. The specimen involves 3,542 random coil molecular chains composed of 500–1500 methylene monomers with about 2 million methylene groups. The stress-strain curve shows a linear elastic relationship at the initial stage of $\varepsilon_{zz} \leq 0.03$ at $\dot{\varepsilon}_{zz} = 5.0 \times 10^{11}$/s. Then the material "yields" by elongating without stress increase up to the strain of 1.5, where strain hardening appears. Careful investigation of changes in dihedral angle and morphology of all molecular chains reveals that the *gauche*→*trans* transition takes place during

yielding, generating a new network-like structure composed of entangled molecular clusters and oriented chains bridging them. The strain hardening is due to the directional orientation and stretching of molecular chains between entanglements in the nucleated structure.

Key words: Molecular Dynamics, Amorphous Polymer, *gauche*↔*trans* Transition, Chain Entanglement, Orientation of Molecular Chain

1 Introduction

Many efforts have so far been made on the development of the constitutive equation that can precisely represent the complex deformation behavior of glassy polymers [1–6]. Some of them have succeeded in producing good agreement with experiments by taking account of the internal microscopic phenomena such as the chain network composed of cross-links, or the physically entangled point of molecular chains. Further details in the micro- to nanoscopic realm, however, cannot be explored by means of continuum approaches based on phenomenological theories on the internal behavior. For further advance in the modelling of glassy polymers, it is of great interest to clarify the mechanism of the chain entanglements and the role of individual chains at the molecular level.

Recent progress in experimental instruments such as TEM tomography [7]

* Corresponding author. Department of Mechanical Engineering, Faculty of Engineering, Kobe University, 1-1, Rokkodai-cho, Nada, Kobe 657-8501, Japan. Tel.:+81-78-803-6303; fax:+81-78-803-6155.
Email address: yashiro@mech.kobe-u.ac.jp (Kisaragi Yashiro).
URL: http://solid.mech.kobe-u.ac.jp/ (Kisaragi Yashiro).

has made it possible to observe the molecular chain structure directly at the molecular level. However, there are still difficulties in sample preparation and observation of the internal deformation process in a time sequence. Computer simulation is a powerful tool for investigating both internal and atomistic phenomena. Among the various computational methods, molecular dynamics simulation may be the best choice for tracing the deformation behavior of individual molecular chains in a time series. With the great advancement of computers, simulations containing over a million atoms with spatial dimensions close to the micrometer level have already been implimented in the studies of plasticity of metallic systems [8–10]. Numerous simulations have also been conducted on the behavior of polymer chains, such as the crystallization process [11–13], structure formation with short molecular chains [14,15], deformation behavior under tension and shear [16–19] and lamella microdomain structure of a copolymer [19]. Shibutani et al. [17,18] have proposed a hierarchical model with many Voigt spring and dashpot pairs of which the elasticity and viscosity are evaluated from the response of amorphous polymer chains in a periodic cell of a molecular dynamics simulation. The coarse-grained molecular dynamics model proposed by Aoyagi et al. [19] is a comprehensive general-purpose program that covers a wide range of molecular modelling, from a full atomistic model to a bead-spring model. These hierarchical models aim to obtain rather macroscopic behavior of numerous segments without an increase in computational cost. There is a possibility, however, of including the artificial and unphysical effects in the scale-up interpretation of the results of atomic-level simulations, such as the determination of segment length or cross-link distance. In fact, Shibutani et al. [18] have faced the problem that the mechanical properties in the atomic simulations are strongly affected by the size of the periodic cell, which is identified by the segment length in their

model, particularly under large strain. For fundamental understanding of the deformation behavior of large, irregular and massive molecular chains in an amorphous polymer, it may still be indispensable to directly trace the motion of all chains with a huge number of molecules.

In the present study, a large molecular dynamics simulation is conducted on a nanoscopic specimen of amorphous polyethylene under tension. The specimen involves 3,542 random coil molecular chains with various lengths of 500-1500 methylene monomers, and the total number of methylene groups reaches about 2 million. By eliminating any periodicity and the chain connecting the top and bottom of the specimen, which undesirably determines the mechanical properties with its "characteristic length", the fundamental mechanism of chain entanglements is investigated in detail.

2 Simulation Procedure

A conventional united atom model, where a CH_2 methylene group is treated as a single particle, is adopted for the present simulation of amorphous polyethylene. The potential energy of the system, $E_{\rm tot}$, is expressed by the sum of the chemical bonding potential (bond stretch, bending, torsion) and the nonbonding potential (van der Waals) between the united atoms as follows;

$$E_{\rm tot} = E_{\rm bs}(r) + E_{\rm be}(\theta) + E_{\rm to}(\phi) + E_{\rm vw}(\bar{r}), \tag{1}$$

where $E_{\rm bs}(r)$ is the 2-body potential for bond length r, $E_{\rm be}(\theta)$ the 3-body potential for bond angle θ, $E_{\rm to}(\phi)$ the 4-body potential for dihedral (torsion) angle ϕ, and $E_{\rm vw}(\bar{r})$ another 2-body potential for nonbonded distance $\bar{r}$. The potential functions and parameters adopted are proposed by Kuwajima et

al. [20] for amorphous polyethelene as shown in the equations below with the parameters listed in Table 1.

$$E_{\rm bs}(r) = \sum \left\{ k_r (r - r_0)^2 \right\} \tag{2}$$

$$E_{\rm be}(\theta) = \sum \left\{ k_\theta (\theta - \theta_0) \right\} \tag{3}$$

$$E_{\rm to}(\phi) = \sum \left\{ V_1 \cos\phi + V_2 \cos 2\phi + V_3 \cos 3\phi + V_6 \cos 6\phi \right\} \tag{4}$$

$$E_{\rm vw}(\bar{r}) = \sum \left\{ A(\bar{r})^{-12} - C(\bar{r})^{-6} \right\} \tag{5}$$

The potential functions of bond stretch and bending are harmonic, of which the equilibrium bond length and angle are $r_0 = 0.1533\,\mathrm{nm}$ and $\theta_0 = 113.3\,\mathrm{deg}$, respectively. The torsion potential is expressed by a cosine polynominal that has a stable point (*trans*) at $\phi = 180\,\mathrm{deg}$ and two metastable points (*gauche*) at $\phi = \pm 67.5\,\mathrm{deg}$. The van der Waals potential is the 12–6 Lennard-Jones type. Summations in Eqs.(2)–(5) are implemented for all nodes.

Figure 1 shows the shape and dimensions of the nanoscopic specimen used in the present study. The specimen has a parallel portion of 50 nm length, a square cross section of 26 nm×26 nm and chuck regions of 5 nm thickness at the top and bottom. The inner structure composed of many random coils is constructed according to the following procedure:

(1) A particle, or a methylene group, is scattered randomly in the body of the specimen as a seed of chain growth.

(2) The chain is grown by the random walk procedure as schematically shown in Fig. 2, in the condition that the bond length and angle are set at r_0 and θ_0, respectively, while the dihedral angle is set at the *trans* or the *gauche* points randomly. It is also permitted for the dihedral angle to deviate from the *gauche* in the range of $\pm 5\,\mathrm{deg}$.

(3) If the front of the chain grown goes out of the specimen, or if the other particles prevent the growth and the chain cannot grow any longer, the chain is terminated at the node. A short chain less than 500 methylene groups is discarded.

The procedure is repeated until the density of the specimen becomes that of the low-density polyethylene, $0.87\,\mathrm{g/cm^3}$. The initial structure generated in the process described above involves 3,542 random coil chains, 500∼1,500 particles per chain and a total number of 1,984,434 particles. There is no chain connecting the top and bottom chuck, thus the chains in chuck region have their ends in the body or at the surface.

The initial structure is relaxed by a molecular dynamics simulation of 3000 fs, restricting the motion of particles in the chuck region within the xy plane. Verlet scheme is adopted for the numerical integration with a time increment of 0.1 fs (10^{-16} sec). After the initial relaxation, tensile simulation up to $\varepsilon_{zz} = 3.0$ is implemented by applying a strain increment of 5.0×10^{-5} at every calculation step, or strain rate of $\dot{\varepsilon}_{zz} = 5.0 \times 10^{11}/\mathrm{s}$. Here, the strain is measured from the initial gauge length of 50 nm. The strain is controlled by expanding the distance between the particles in the z-direction proportionally. The temperature is kept at 300 K by velocity scaling during the simulations.

3 Results and Discussion

3.1 Initial equilibrium structure and yield

Figure 3 shows the distributions of bond length, bending angle, torsion angle and local density in the equilibrium state after the initial relaxation. The local density is defined in the present study as the density evaluated by the number of atoms in a sphere, of radius 8 nm or the cut-off distance of Eq.(5), centered at the position of the target particle. The distribution of bond length and angle shows a pulse-like sharp peak at the position of r_0 and θ_0, implying almost every node is at the equilibrium length and angle. The torsion angle also has its peaks at the stable and metastable points of *trans* and *gauche*, however, there are many nodes deviated from the stable or metastable angle so that the peaks have broader bases. This implies the potential energy of the whole system is minimum by the initial relaxation but some torsion angles remain at the high energy state in the intricated amorphous chain structure. The atomic density has its peak at the controlled density of $0.87\,\mathrm{g/cm^3}$ and a wide distribution in the lower side due to the surfaces.

The nominal stress–nominal strain curve at the initial stage of straining is shown in Fig. 4. The stress is evaluated with the z-component of the force acting on the particles in the top and bottom chucks and the cross-sectional area of the parallel portion. It shows a linear elastic relationship up to the strain of 0.012, where the stress decreases slightly and makes a small peak as indicated by Arrow ①. Then the stress increases again and shows the maximum peak of $\sigma_{zz} = 0.92\,\mathrm{GPa}$ at $\varepsilon_{zz} = 0.027$ (Arrow ②). After this peak the curve becomes flat with little oscillation while the strain continues to

increase.

Figure 5 illustrates the change in the potential energy of the system, E_{tot}, and its components, $E_{\mathrm{bs}}, E_{\mathrm{be}}, E_{\mathrm{to}}$ and E_{vw}, corresponding to Fig. 4. The ordinate is the difference between the value at each strain and that in the initial equilibrium, for comparing the changes of each component in the same order. Lines ① and ② indicate the strains corresponding to the two peaks of Arrows ① and ② in Fig. 4. The strain of both Lines ① and ② coincides with the (local) maximum of bending potential and almost the local minimum of the bond stretch. It is noteworthy that an energy exchange takes place before each peak of ① and ②, that is, the bending increases to decrease the primarily increased bond stretch, without significant change in stress. All these suggest the following mechanisms of the internal change before and after the stress peak: (1) the small variation of bond stretch absorbs the deformation primarily, (2) the energy exchange occurs between the bond stretch and bending, by changing the bending angle to relax the bond stretch at its limit, and (3) the stress begins to decrease when the bending change cannot absorb the deformation anymore. Here, the important fact that the torsion potential shows prominent change at each peak, rapid drop at Peak ① and a minimum at Peak ②, suggests that the dihedral rotation plays an important role in the stress decrease. Detailed investigation on the change of all dihedral nodes reveals that the rotation of the dihedral angle observed during ① and ② is within $\pm 30\,\mathrm{deg}$ while that after ② exceeds $\pm 60\,\mathrm{deg}$, resulting in the *gauche* $\Leftrightarrow$ *trans* transition. This leads to the following conclusion on the internal change at the peaks: (i) The change at ① is the relaxation of the dihedral angles, which have higher energy in the initial equilibrium structure, by the driving force of the applied strain. (ii) The change at ② is the conformational change of molecular chains to relax

the bending angle strained.

3.2 Yield ⇒ hardening behavior

The overall stress–strain curve up to the strain of 3.0 is shown in Fig. 6. After the initial yield described in the previous section, the material elongates without significant stress increase until the strain of about 1.5, showing stress fluctuation. On the other hand, stress prominently increases after $\varepsilon_{zz} = 1.5$ just like the strain hardening observed in the macroscopic tension test. They are not related directly to each other since there is a significant difference in time and spatial scale, however, we will refer to the region of $\varepsilon_{zz} \leq 1.5$ as the "yield region" and that of $\varepsilon_{zz} > 1.5$ as the "strain hardening region" from the similarity of the stress–strain curve.

Figure 7 shows the change in the potential components associated with Fig. 6. In the yield region, only the torsion shows remarkable change at $\varepsilon_{zz} = 0.5$, where it turns to decrease, while the bond stretch and bending increase monotonically. The torsion becomes lower than the initial equilibirum at the beginning of the strain hardening, $\varepsilon_{zz} = 1.5$. This implies the significant structure change occurs in the internal molecular chains during the yield ⇒ hardening process. Figure 8 illustrates the number of dihedral nodes that show *gauche* ⇒ *trans* or *trans* ⇒ *gauche* transition by rotating over ±60 deg. In the region of $\varepsilon_{zz} \leq 0.5$, the *trans* ⇒ *gauche* transition looks flat around 4,000 ∼ 4,500 while the *gauche* ⇒ *trans* transition decreases monotonically. This is because the increment of *trans* nodes with the *gauche* ⇒ *trans* transition, that decreases the system energy, are subtly balanced with the probability of the *trans* ⇒ *gauche* transition, that increases the energy. Then, the number

of *gauche* nodes decreases and that of *trans* increases after $\varepsilon_{zz} = 0.5$, from the fact that both transitions decrease monotonically and the *gauche* $\Rightarrow$ *trans* transition is twice as much as the other. This implies the inner molecular chains become straight from $\varepsilon_{zz} = 0.5$.

3.3 Chain entanglements and directional orientation

Figure 9 shows the snapshots of molecular chains in the tensile simulation. In the figure, a rectangular region in the center of the specimen, of which initial size is 10 nm $\times$ 10 nm $\times$ 3 nm, is drawn. The black particles indicate the flexion nodes at the initial equilibrium, as described later. The material deforms homogeneously and maintains the initial chain structure until $\varepsilon_{zz} = 0.5$, however, a few voids appear in contrast with the deformation of an amorphous metal [21]. The inhomogeneity in the density becomes clearer in the figure with $\varepsilon_{zz} = 1.0$, where splitting clusters of molecular chains with voids can be observed. Here, we can see straightened chains notably in the low-density regions, or the void regions between clusters. At the beginning of the strain hardening at $\varepsilon_{zz} = 1.5$, a new network structure is generated where long straightened chains connect the clusters of entangled chains. It is also observed that many chains between clusters are oriented in the tensile direction. After a strain of 1.5, some clusters dissolve but the material deforms mainly by the stretching of the oriented chains between clusters keeping the generated network structure, as recognized from the positions of clusters I and II in the figures with $\varepsilon_{zz} = 1.5 \sim 3.0$. It should be concluded from these facts that the stress increase in the present simulation, where no chain connects the top and bottom of the specimen, is caused by the nucleation of the network

chain structure with the "entanglements" and the orientation and stretch of the chains bridging them.

In order to clarify the characteristics of the entanglements at the initial equilibrium state, the "flexion nodes" in all molecular chains are investigated. As schematically illustrated in Fig. 10, the interior angle between two position vectors from the target particle A to the particles B and C, 10 backward and forward monomers, are evaluated. The particles, at which the angle is less than 90 deg at the initial equilibrium, are drawn in black in Fig. 9 as flexion nodes. Dense flexion nodes can be observed at the entanglements in the figure with $\varepsilon_{zz} = 3.0$, thus it is suggested that the flexion nodes tend to make entanglements. It is also pointed out, however, that there are many flexion nodes straightened during the deformation, since many black particles can be seen in the long straightened chains. From these remarks and the figure of $\varepsilon_{zz} = 0.0$, we can see that the initial arrangement of the dense flexion nodes does not correlate well with the entanglements nucleated during the yield $\Rightarrow$ hardening process. The configuration or distance of the entanglements, of great interest from the viewpoint of hierarchical modelling, may not be easily characterized by the initial chain structure but depends on the history of complicated local deformations.

The change in the distribution of local density during the yield $\Rightarrow$ hardening process is shown in Fig. 11. In the figures with $\varepsilon_{zz} = 0.5$ and 1.0, the peak translates to the lower side by tension, however, the distribution maintains a broad base at the higher side because of the clusters shown in Fig. 9. It is confirmed quantitatively from the figure with $\varepsilon_{zz} = 1.5$ that a new structure nucleates at the beginning of the strain hardening, since another small peak appears near $\rho = 0.53\,\mathrm{g/cm^3}$ in the density distribution. Figure 12 illustrates

particles with a higher local density than the branched peak, ρ_{high}, at each strain of 1.5∼3.0. Clusters A, B and C are indicated by ellipsoids in the figure as an example to make the relative position of the clusters clear. Many of the entanglements are observed in the center of the cross section, a few at the surface, and none at the corners. Most of the entangled chains at the corners and surfaces have disappeared during the yield ⇒ hardening process, since they can be more easily dissolved than those inside. The characteristic distance between the entanglements could not be decided quantitatively, since they disperse widely as can be seen in the figure. The relationship between the distance and the average molecular weight remains to be invesitigated statistically in the next study.

4 Conclusive Remarks

In order to clarify the fundamental mechanism of deformation behavior of irregular and massive random coil molecular chains in amorphous polymers, a molecular dynamics simulation is conducted on the nanoscopic specimen of amorphous polyethylene under tension. The results are summarized as follows:

(1) After showing the linear elastic response at the initial stage of straining, the material yields by elongating without significant stress increase at $\dot{\varepsilon}_{zz} = 5.0 \times 10^{11}/\text{s}$. Then the material shows strain hardening at $\varepsilon_{zz} > 1.5$, increasing the stress prominently.

(2) The change in the potential energy from the linear elastic to the yield reveals the internal mechanism as follows; (a) small variation of bond stretching absorbs the deformation primarily, (b) bending angles begin to change when the deformation by bond stretching reaches the limit,

(c) finally the dihedral angles rotate to relax the stress increased.

(3) It is also suggested from the change in the dihedral angles that chains become straight during the yield process since the *gauche* $\Rightarrow$ *trans* transitions predominantly take place.

(4) The chain morphology and the distribution of local density show that a new network structure, where the clusters of the entangled chains are connected with the straightened chains, nucleates during the yield $\Rightarrow$ hardening process.

(5) It is concluded that the stress increase at $\varepsilon_{zz} > 1.5$ in the present simulation, where no chain connects the top and bottom of the specimen, is caused by the nucleation of the network chain structure with the "entanglements" and the orientation and stretch of the chains bridging them.

The structural change of molecular chains such as chain folding requires more time in real polymetric materials. Thus it is true that there is still a large difference particularly in the time scale, between the mechanism presented and the phenomena in real materials. On the time dependent behavior of molecular chains, further investigation using the molecular dynamics based on transition state theory [22,23] is desired for future work.

Acknowledgements

This work was supported financially in part by a Grant-in-Aid for Scientific Research from the Ministry of Education, Culture, Sports, Science and Technology of Japan.

References

[1] Argon, A. S., A theory for the low-temperature plastic deformation of glassy polymers, Philosophical Magazine, **28** (1973), 839–865.

[2] Boyce, M. C., Parks, D. M., Argon, A. S., Large inelastic deformation of glassy polymers, Part I: rate dependent constitutive model, Mechanical Materials, **7** (1988), 15–33.

[3] Arruda, E. M., Boyce, M.C., A three-dimensional constitutive model for large stretch behavior of rubber mateials, *Journal of the Mechanics and Physics of Solids*, **41** (1993), 389–412.

[4] Wu, P. D., Van der Giessen, E., On improved network models for rubber elasticity and their applications to orientation hardening in glassy polymers, it Journal of the Mechanics and Physics of Solids, **41** (1993), 427–456.

[5] Tomita, Y., Tanaka, S., Prediction of deformation behavior of glassy polymers based on molecular chain network model, Internatonal Journal of Solids Structures, **32** (1995), 3423–3434.

[6] Tomita, Y., Adachi, T., Tanaka, S., Modelling and application of constitutive equation for glassy polymer based on nonaffine network theory, European Journal of Mechanics A Solids, **16** (1997), 745–755.

[7] Furukawa, H., Shimizu, M., Suzuki, Y. and Nishioka, H., System for three-dimensional reconstruction of TEM images based on computerized tomography method, JEOL News, **36**, No.1, (2001), 50–55.

[8] Abraham, F. F., Atomistic Simulations of Crack Propagation, Materials Science for the 21st Century, Vol.A, (2001), 195–202, The Society of Materials Science, Japan.

[9] Vashishta, P., Bachelechener, M. E., Nakano, A., Campbell, T. J., Kalia, R. K., Kodiyalam, S., Ogata, S., Shimojo, F., Walsh, P., Multimillion atom simulation of mechanical behavior of nanostructured materials, interfaces, and dynamics oxidation, Materials Science for the 21st Century, Vol.A, (2001), 213–219, The Society of Materials Science, Japan.

[10] Yashiro, K., Naito, M., Tomita, Y., Molecular Dynamics Simulation of Dislocation Nucleation and Motion at γ/γ' Interface in Ni-Based Superalloy, International Journal of Mechanical Sciences, **44**–9 (2002), 1845–1860.

[11] Kavassalis, T., A., Sundarajan, P., R., Molecular dynamics study of polyethylene crystallization, Macromolecules, **26** (1993) 4144–4150.

[12] Yamamoto, T., Molecular dynamics simulation of polymer ordering I. Crystallization from vapor phase, The Journal of Chemical Physics, **108** (1998), 4638–4645.

[13] Yamamoto, T., Molecular dynamics simulation of polymer ordering. II. Crystallization from the melt, The Journal of Chemical Physics, **115** (2001) 8675–8680.

[14] Fujiwara, S., Sato, T., Physcal Review Letters, **80** (1998), 991–994.

[15] Fujiwara, S., Sato, T., Molecular dynamics simulation of structure formation of short chain molecules, The Journal of Chemical Physics, **110**–19 (1999), 9757–9764.

[16] Ogura, I., Yamamoto, T., Molecular dynamics simulation of large deformation in an amorphous polymer, Polymer, **36** (1995), 1375-1381.

[17] Shibutani, Y., Nakamura, K., Tomita, Y., Free energy change of amorphous polymer structure under uniaxial tension, Transaction of the Japan Society of Mechanical Engineers, Series A, **65**–629 (1999), 87–92. (in Japanese)

[18] Ichiyanagi, J., Research about the Hierarchical Modeling of Amorphous Polymer, Solid Mechanics Research Report, No.0010 (2000). (in Japanese)

[19] Aoyagi, T., Sawa, F., Shoji, T., Fukunaga, H., Takimoto, Jun-ichi, Doi, M., A general-purpose coarse-grained molecular dynamics program, Computer Physics Communications, **145** (2002), 267–279.

[20] Kuwajima, S., Noma, H., Ohsaka, T., Proceedings of the 4th symposium of the society of computer chemistry, Japan (1994), 53–56. (in Japanese)

[21] Matsumoto, R., Kitagawa, H., Nakatani, K., Nakatani, A., Molecular dynamics simulation on a crack propagating in amorhous metal, Transaction of the Japan Society of Mechanical Engineers, Series A **76**–653 (2001), 23–29. (in Japanese)

[22] A. F. Voter, A method for accelerating the molecular dynamics simulation of infrequent events, The Journal of Chemical Physics, **106** (1997), 4665–4677.

[23] D. S. Christopher , N. Houbi, S. P. Vijay, G. Martin, Absolute comparison of simulated and experimental protein-folding dynamics, Nature, **420**–7 (2002), 102–106.

Captions.

Table 1

Potential parameters for polyethylene.

Fig. 1. Schematic of the nanoscopic specimen and dimensions.

Fig. 2. Modeling of random coil molecular chain.

Fig. 3. Distribution in bond stretch, bending angle, torsion angle and atomic density.

Fig. 4. Change in tensile stress at the initial stage of the tensile simulation ($\varepsilon_{zz} \leq 0.08$).

Fig. 5. Change in potential energy at the initial stage of the tensile simulation ($\varepsilon_{zz} \leq 0.08$).

Fig. 6. Change in tensile stress in the tensile simulation up to the strain of $\varepsilon_{zz} = 3.0$.

Fig. 7. Change in potential energy in the tensile simulation up to the strain of $\varepsilon_{zz} = 3.0$.

Fig. 8. Change in the number of dihedral nodes showing *gauche* $\Leftrightarrow$ *trans* transitions.

Fig. 9. Snapshots of molecular chains.

Fig. 10. Schematic of evaluation of flexion node.

Fig. 11. Change in distribution of atomic density.

Fig. 12. Entanglements evaluated by particles of high atomic density.

Table 1.

r_0 [nm]	0.1533
k_r [kJ/(mol·nm^2)]	1.373×10^5
θ_0 [deg.]	113.3
k_θ [kJ/(mol·rad^2)]	374.7
V_1 [kJ/mol]	3.935
V_2 [kJ/mol]	2.177
V_3 [kJ/mol]	7.786
V_6 [kJ/mol]	0.0
A [kJ/mol·nm^{12}]	2.972×10^{19}
C [kJ/mol·nm^6]	6.907×10^9

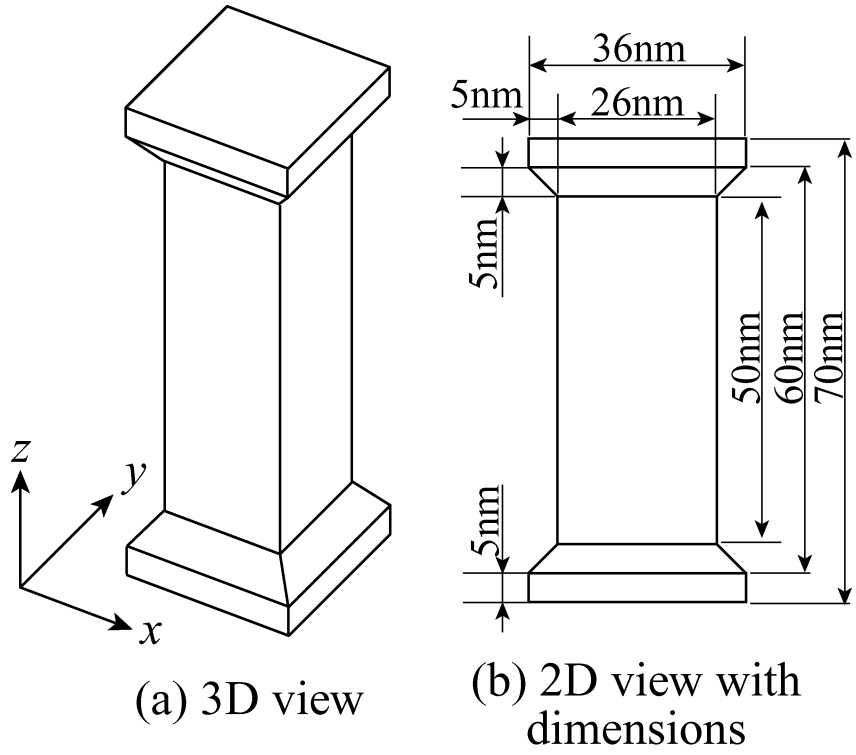
z
y
x
36nm
5nm
26nm
5nm
50nm
60nm
70nm
5nm
(a) 3D view
(b) 2D view with dimensions

Figure 1

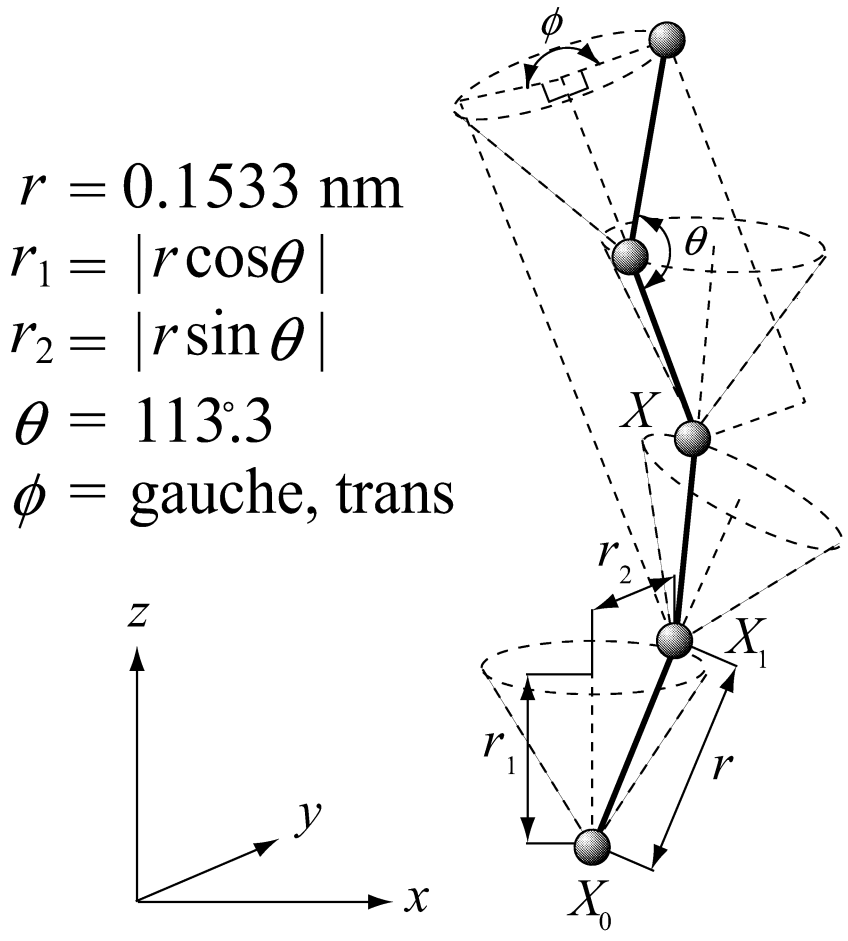
$r = 0.1533$ nm
$r_1 = |r\cos\theta|$
$r_2 = |r\sin\theta|$
$\theta = 113.3°$
ϕ = gauche, trans
ϕ
θ
X
r_2
X_1
r_1
r
X_0
z
y
x

Figure 2

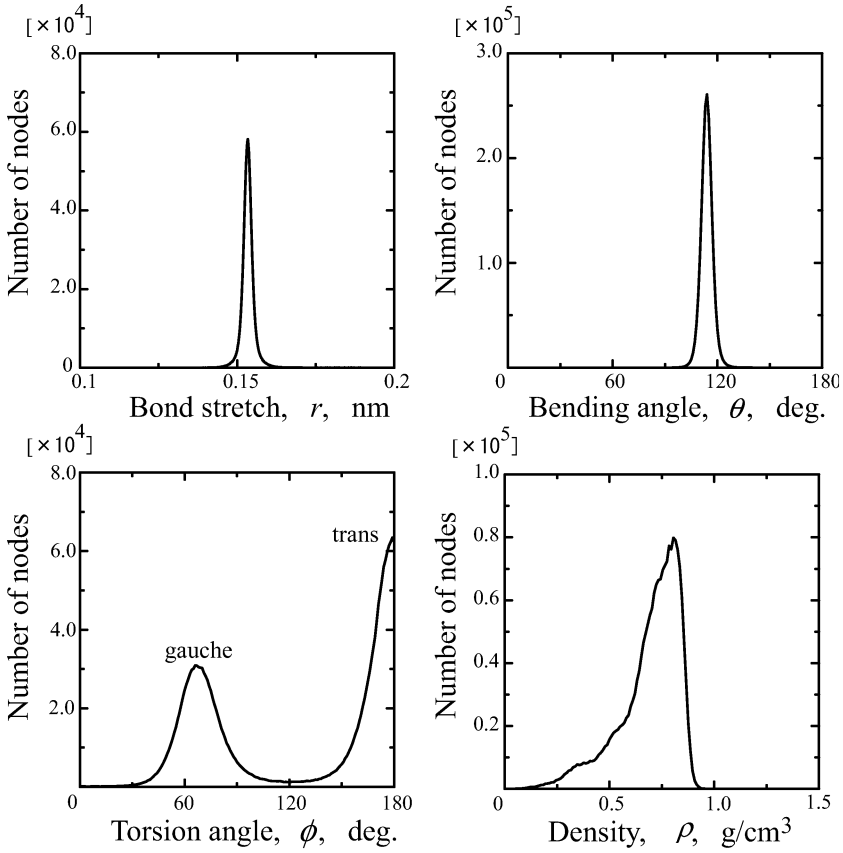
[×10^4]
Number of nodes
8.0
6.0
4.0
2.0
0
0.1
0.15
0.2
Bond stretch, r, nm
[×10^5]
Number of nodes
3.0
2.0
1.0
0
60
120
180
Bending angle, θ, deg.
[×10^4]
Number of nodes
8.0
6.0
4.0
2.0
trans
gauche
0
60
120
180
Torsion angle, φ, deg.
[×10^5]
Number of nodes
1.0
0.8
0.6
0.4
0.2
0
0.5
1.0
1.5
Density, ρ, g/cm3

Figure 3

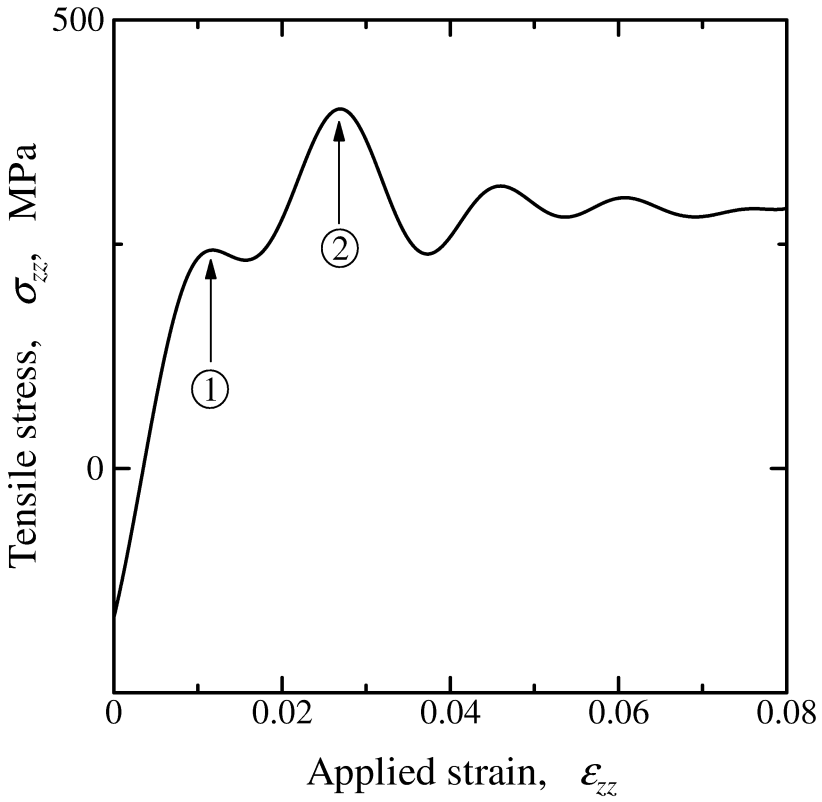
500
0
Tensile stress, σ_{zz}, MPa
①
②
0
0.02
0.04
0.06
0.08
Applied strain, ε_{zz}

Figure 4

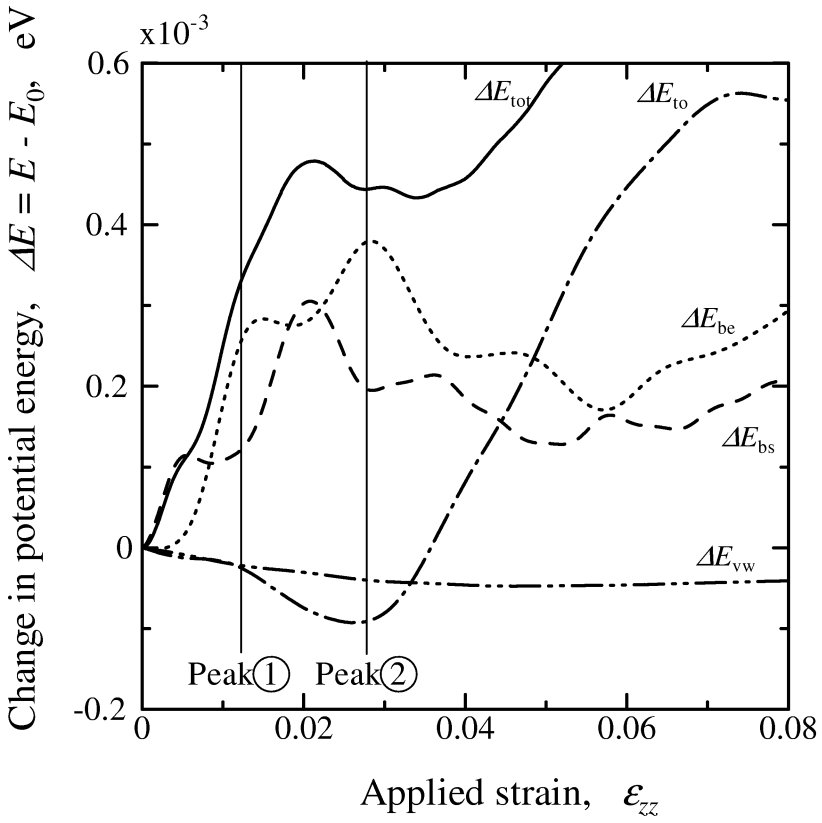
x10^-3
0.6
0.4
0.2
0
-0.2
0
0.02
0.04
0.06
0.08
Change in potential energy, ΔE = E - E0, eV
Applied strain, εzz
ΔEtot
ΔEto
ΔEbe
ΔEbs
ΔEvw
Peak① Peak②

Figure 5

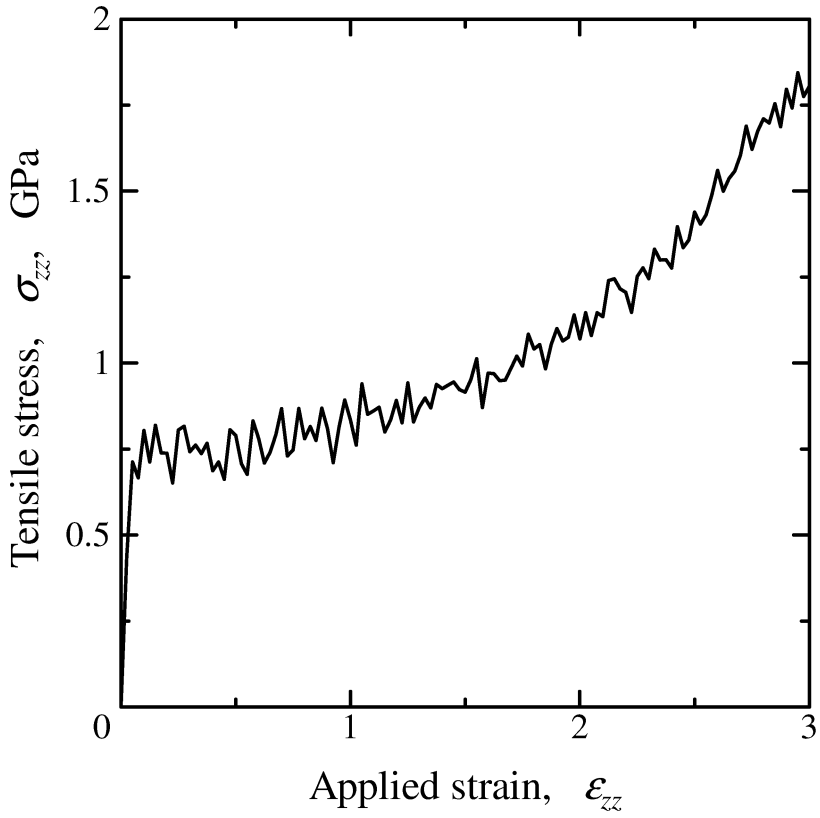
Tensile stress, σ_{zz}, GPa
Applied strain, ε_{zz}
0
0.5
1
1.5
2
0
1
2
3

Figure 6

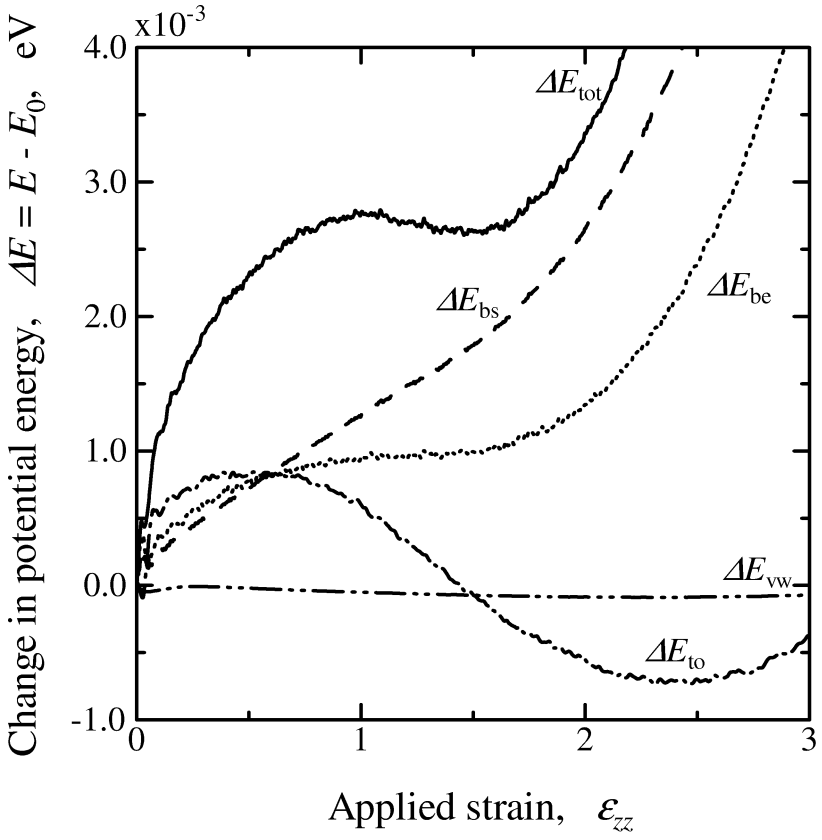
x10^-3
4.0
3.0
2.0
1.0
0.0
-1.0
0
1
2
3
ΔE_tot
ΔE_bs
ΔE_be
ΔE_vw
ΔE_to
Change in potential energy, ΔE = E - E_0, eV
Applied strain, ε_zz

Figure 7

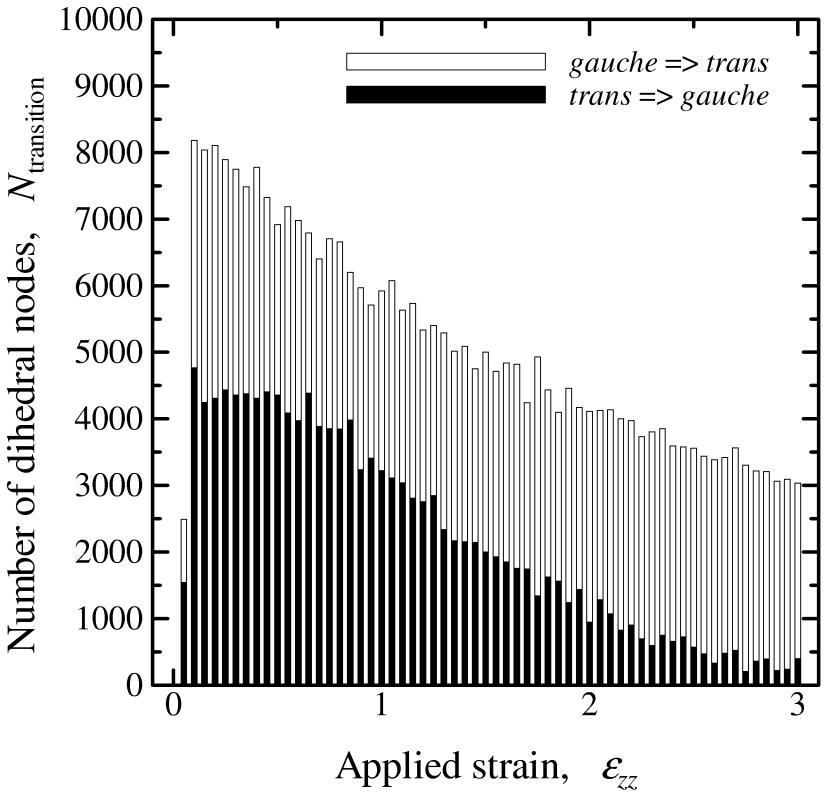
10000
9000
8000
7000
6000
5000
4000
3000
2000
1000
0
0
1
2
3
gauche => trans
trans => gauche
Number of dihedral nodes, $N_{transition}$
Applied strain, ε_{zz}

Figure 8

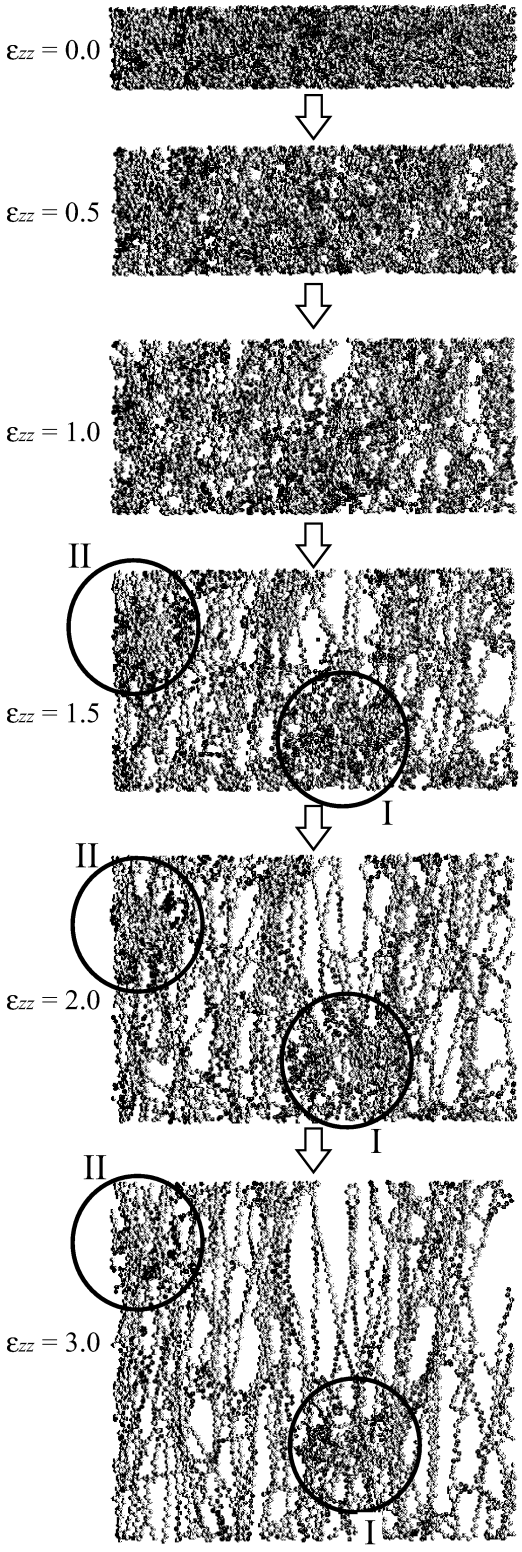

Figure 9

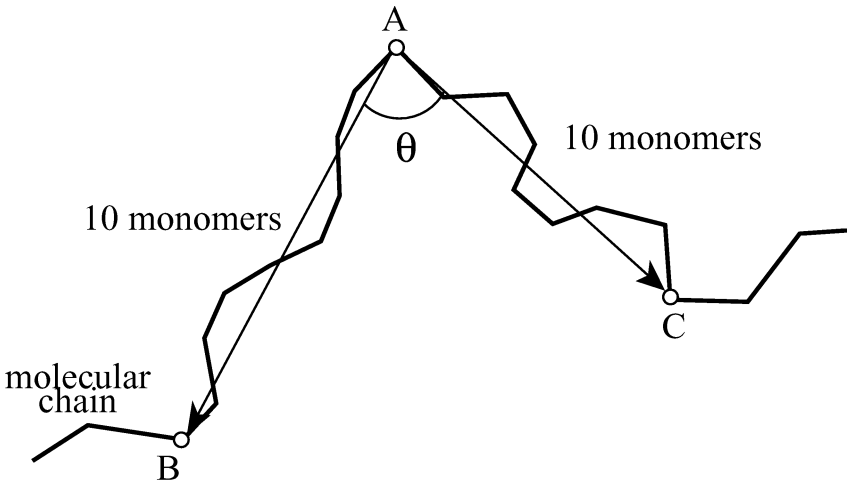

Figure 10

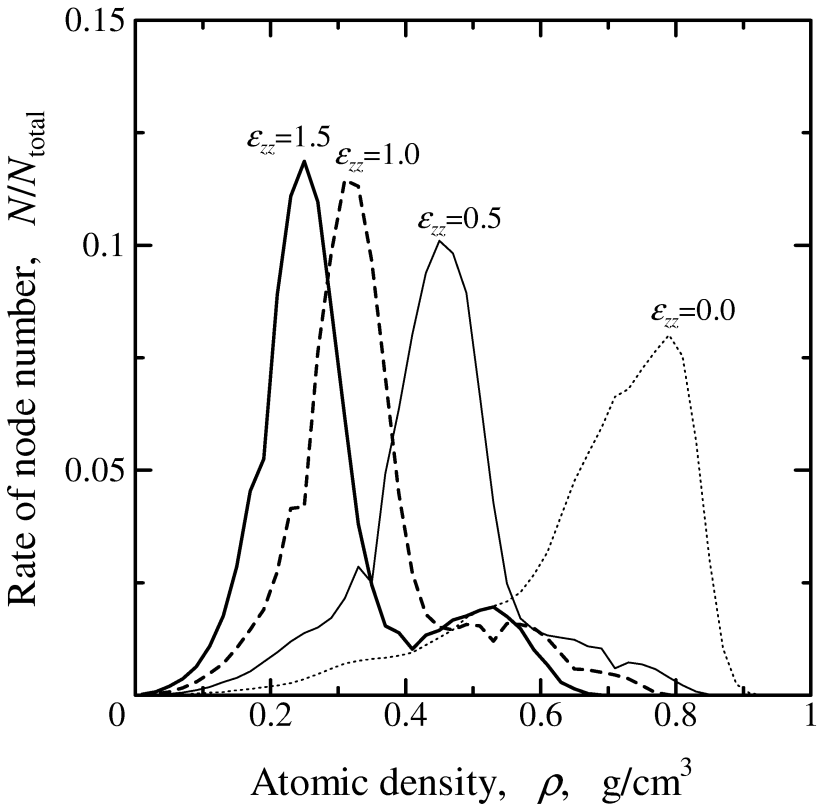
0.15
0.1
0.05
0
0.2
0.4
0.6
0.8
1
Rate of node number, N/N_{total}
Atomic density, ρ, g/cm^3
ε_{zz}=1.5
ε_{zz}=1.0
ε_{zz}=0.5
ε_{zz}=0.0

Figure 11

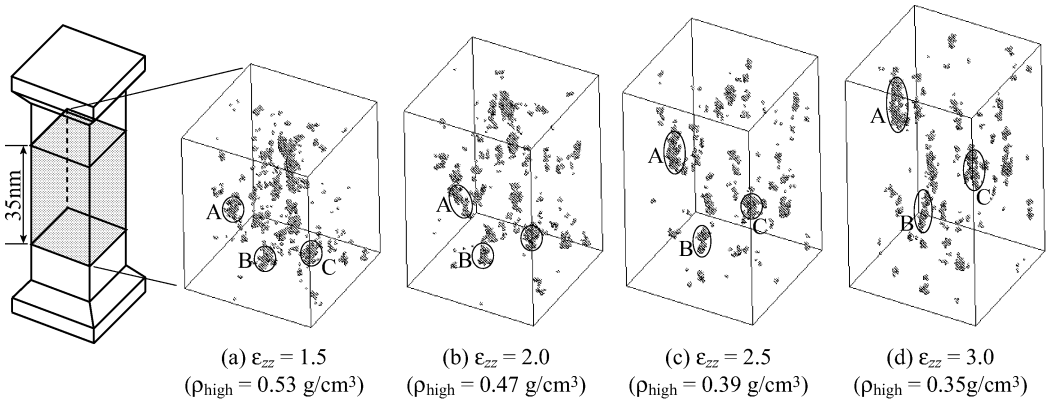

(a) $\varepsilon_{zz} = 1.5$ ($\rho_{high} = 0.53$ g/cm^3)
(b) $\varepsilon_{zz} = 2.0$ ($\rho_{high} = 0.47$ g/cm^3)
(c) $\varepsilon_{zz} = 2.5$ ($\rho_{high} = 0.39$ g/cm^3)
(d) $\varepsilon_{zz} = 3.0$ ($\rho_{high} = 0.35$g/cm^3)

Figure 12